JACS
JOURNAL OF THE AMERICAN CHEMICAL SOCIETY
Communication
pubs.acs.org/JACS

Tackling CO Poisoning with Single-Atom Alloy Catalysts

Jilei Liu,[†,⊥] Felicia R. Lucci,[‡,⊥] Ming Yang,[†] Sungsik Lee,[§] Matthew D. Marcinkowski,[‡] Andrew J. Therrien,[‡] Christopher T. Williams,[∥] E. Charles H. Sykes,*[,‡] and Maria Flytzani-Stephanopoulos*[,†]

[†]Department of Chemical and Biological Engineering, Tufts University, 4 Colby Street, Medford, Massachusetts 02155, United States
[‡]Department of Chemistry, Tufts University, 62 Talbot Avenue, Medford, Massachusetts 02155, United States
[§]X-ray Science Division, Argonne National Laboratory, 9700 South Cass Avenue, Argonne, Illinois 60439, United States
[∥]Department of Chemical Engineering, University of South Carolina, 301 Main Street, Columbia, South Carolina 29208, United States

Supporting Information

ABSTRACT: Platinum catalysts are extensively used in the chemical industry and as electrocatalysts in fuel cells. Pt is notorious for its sensitivity to poisoning by strong CO adsorption. Here we demonstrate that the single-atom alloy (SAA) strategy applied to Pt reduces the binding strength of CO while maintaining catalytic performance. By using surface sensitive studies, we determined the binding strength of CO to different Pt ensembles, and this in turn guided the preparation of PtCu alloy nanoparticles (NPs). The atomic ratio Pt:Cu = 1:125 yielded a SAA which exhibited excellent CO tolerance in H_2 activation, the key elementary step for hydrogenation and hydrogen electro-oxidation. As a probe reaction, the selective hydrogenation of acetylene to ethene was performed under flow conditions on the SAA NPs supported on alumina without activity loss in the presence of CO. The ability to maintain reactivity in the presence of CO is vital to other industrial reaction systems, such as hydrocarbon oxidation, electrochemical methanol oxidation, and hydrogen fuel cells.

Platinum is widely used for fuel cell anodes and hydrocarbon processing due to its superior catalytic performance. Pt metals are highly active for H_2 dissociation but are very susceptible to carbon monoxide (CO) poisoning.[1] Due to its strong binding to Pt, even trace amounts of CO impurity, which is always present in H_2 gas produced from fuel reforming, can diminish H_2 activation and reactivity.[2] This strong CO adsorption also hinders the fast conversion of CO to CO_2 at low temperatures (<200 °C), and becomes a technical challenge for efficient emission control and water−gas shift (WGS) for hydrogen upgrading. Recently, atomically dispersed Pt_1 (or Pd_1)-O_x- stabilized on a variety of supports, such as silica,[3] titania,[4] KLTL-Zeolite,[4,5] MCM-41,[4] alumina,[6] and iron oxide,[7] was found to be highly active in WGS and CO oxidation reactions, and $Pd_1/g\text{-}C_3N_4$ was reported to be active and stable in the selective hydrogenation of 1-hexyne to 1-hexene.[8] The single-atom Pt sites have a cationic nature that results in weak CO adsorption,[3] thus making them the exclusive sites for the low-temperature CO conversion. Although single-atom catalytic sites in Pt_1 (or Pd_1)-O_x-oxides possess the desired property of weaker CO adsorption, they may not be stable enough under hydrogenation conditions.

Alternatively, single-atom alloy (SAA) catalysts were also shown to be active for a variety of selective hydrogenation[9−11] and dehydrogenation reactions,[12,13] including the Pd-Cu SAA for the selective hydrogenation of styrene,[9] acetylene,[9] and phenylacetylene.[10] Moreover, the Pt-Cu SAA was shown by Lucci et al. to selectively hydrogenate 1,3-butadiene to butene under realistic flow reactor conditions.[11] For Pt-Cu SAAs, H_2 dissociation occurs at the single-atom Pt sites, followed by spillover of atomic hydrogen to the Cu surface, where selective hydrogenation takes place.[11,14] Both Pt-Cu(111) SAAs in ultrahigh vacuum (UHV) and Pt-Cu SAA nanoparticle (NP) catalysts in flow conditions at 1 bar exhibit highly selective and stable butadiene hydrogenation reactivity.[11] As a natural expansion of the SAA concept, herein we tackle the issue of CO poisoning of Pt catalysts with Pt-based SAAs in which the Pt atoms are embedded in a host metal surface, such as Cu. The situation for isolated Pt atoms may be different than that for traditional bimetallic alloys, where ensemble effects have been shown to increase the CO binding strength at extended catalytic metal sites.[15−17] From a fundamental perspective, metal alloys that alter the adsorption geometry of CO can exhibit weaker CO binding and enhanced CO tolerance. Isolated Pt atoms enable exclusively atop adsorption configuration of CO, which we show is weaker than CO adsorption on extended Pt sites. Herein, we investigate the interaction between CO and Pt sites on a Pt-Cu SAA and demonstrate improved CO tolerance of Pt-Cu SAA catalysts under realistic working conditions for H_2 activation and acetylene hydrogenation reaction.

By using model Pt-Cu SAAs, we first determined the binding strength of CO to isolated Pt atoms on the surface of Cu(111) (Figure 1A). Weakly bound CO desorbs from Cu(111) below 200 K, and after deposition of 0.01 ML Pt, a CO desorption peak was observed in temperature-programmed desorption traces at 350 K. At an increased coverage of 0.3 ML Pt, CO desorbed at 360 K, with a high-temperature tail. The high-

Received: March 31, 2016
Published: May 11, 2016

DOI: 10.1021/jacs.6b03339
J. Am. Chem. Soc. 2016, 138, 6396−6399

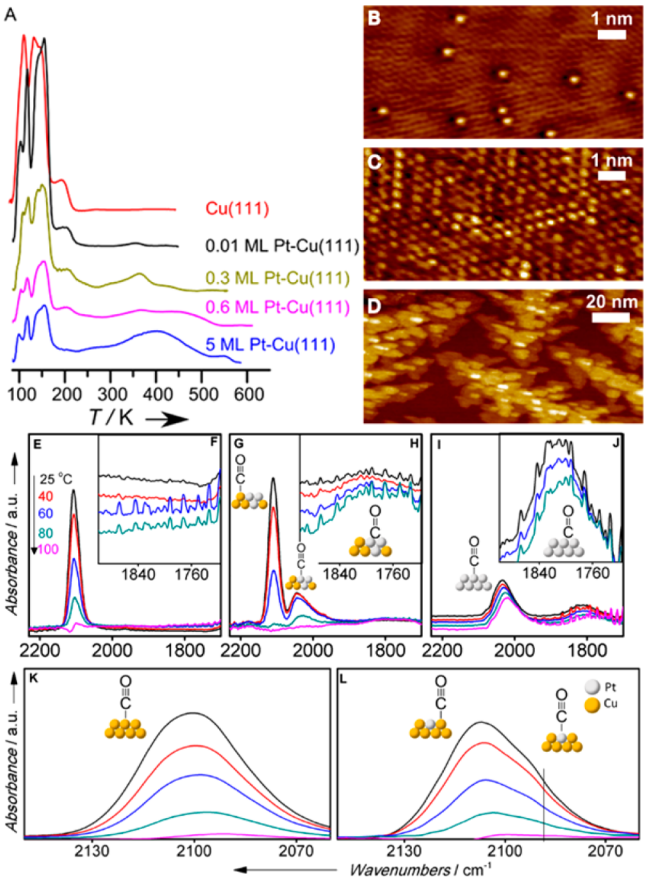

Figure 1. Binding strength of CO to Pt-Cu SAAs vs pure Pt. (A) CO desorption and STM images of (B) 0.01 ML, (C) 0.3 ML, and (D) 1 ML Pt-Cu(111) alloys prepared at 380 K. Scanning conditions: (B) −10 mV and 150 nA; (C) −10 mV and 250 nA; (D) 500 mV and 10 nA. IR spectra in the carbonyl range of pre-reduced (E,F,L) $Pt_{0.008}$Cu-SAA, (G,H) $Pt_{0.39}$Cu-bimetallic, (I,J) Pt-NP, and (K) Cu-NP.

temperature tail developed into an additional peak at 480 K at a Pt coverage of 0.6 ML. At 5 ML, a desorption feature was observed at 410 K, and the surface is assumed to be terminated as Pt(111).

In agreement with the Pt surface structure observed by scanning tunneling microscopy (STM),[14,18] the CO desorption traces reveal the development of three distinct Pt-Cu alloyed structures with increasing Pt coverage (Figure 1B−D). With atomic resolution, the Pt atoms image ∼20 pm taller than the surrounding Cu lattice and appear as brighter protrusions. At low Pt coverages, CO desorbs from isolated Pt atoms (peak at 350 K), and at intermediate coverages, CO desorbs from extended ensembles of Pt atoms (peak at 480 K). At 5 ML Pt, the surface layer is composed primarily of continuous ordered Pt atoms, and CO desorbs at 410 K. At low CO coverages, CO desorption from Pt(111) is reported at 450 K, and with increasing CO coverage desorption is observed at 400 K due to the repulsion between co-adsorbed CO molecules.[19] In Pt-Cu alloys, CO adsorbs weakest on the Pt-Cu SAA and strongest on the extended Pt clusters.

To apply this surface science and microscopy knowledge to the design of heterogeneous catalysts, Pt-Cu alloy NPs were prepared by galvanic replacement of Pt for Cu on preformed Cu NPs (Table S1).[10,11] $Pt_{0.008}$Cu supported on γ-Al_2O_3 is a SAA, as confirmed by aberration-corrected high-angle annular dark field scanning transmission electron microscopy and extend X-ray absorption fine structure (EXAFS) studies.[11] Importantly, with CO in the gas phase, no Pt−Pt interactions were found by EXAFS in $Pt_{0.008}$Cu-SAA (Table S2, Figure S5), which demonstrates the stability of the isolated Pt atoms in the presence of CO.

The binding strength of CO on Pt-Cu alloys and their monometallic counterparts in NP forms was investigated at ambient pressure by IR spectroscopy. Signals for CO bridged-adsorbed to two adjacent Pt atoms between 1900 and 1700 cm^{-1} were observed on the Pt-NP and $Pt_{0.39}$Cu-bimetallic but not seen on the $Pt_{0.008}$Cu-SAA (Figure 1F,H,J). This is consistent with the fact that exclusively isolated Pt atoms are on the surface of $Pt_{0.008}$Cu-SAA, unlike the existence of a mixed phase of Pt atoms, clusters, and particles on the Pt-NP and $Pt_{0.39}$Cu-bimetallic. Overlapping peaks between 2150 and 2060 cm^{-1} are seen for $Pt_{0.008}$Cu-SAA, as indicated by the asymmetric absorption band (Figure 1L). The unique absorption band centered at ca. 2088 cm^{-1} is distinct from atop CO on the Cu or Pt NPs and is assigned to the linearly adsorbed CO on the isolated single Pt atoms. The absorption band of linearly adsorbed CO is at ca. 2020 cm^{-1} on Pt-NP, 2031 cm^{-1} on the Pt ensembles on $Pt_{0.39}$Cu-bimetallic, and 2093 cm^{-1} on Cu-NP (Figure 1G,I,K). As for the different Pt species characterized by CO-IR, their formal charges and coordination numbers are essentially the same, and dipole−dipole coupling has little effect on $Pt_{0.008}$Cu-SAA due to the weak CO−metal bonds on isolated Pt atoms and Cu surfaces.[20] Hence, the strength of CO binding indicates the relative CO−metal π backbonding strength, that is, the stronger the CO−metal bond, the lower the C−O vibrational frequency. We conclude that Pt−CO bonds are weakest on $Pt_{0.008}$Cu-SAA and strongest on Pt-NP, while the Pt cluster in $Pt_{0.39}$Cu-bimetallic has an intermediate binding strength for CO. Moreover, the adsorption strength of CO on the $Cu_3Pt(111)$ alloy is lower than that on Pt(111) according to DFT calculations.[21]

To probe the interaction of CO and H with the Pt catalytic sites at the atomic scale, H and CO were co-adsorbed onto 0.01 ML Pt-Cu(111) (Figure 2). We used the STM tip to interrogate the nature of the H and CO adsorption sites.

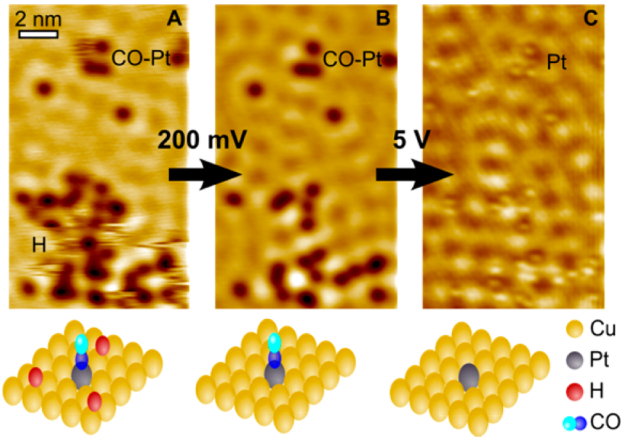

Figure 2. STM images showing the co-adsorption of H and CO on a Pt-Cu(111) SAA surface and STM tip-induced adsorbate removal to reveal the binding sites beneath. (A) H and CO adsorbed on Pt-Cu(111) SAA. (B) Image of same area following scanning at 200 mV to remove adsorbed H. (C) After 5 V pulses to remove adsorbed CO, individual Pt atoms are seen underneath each removed CO molecule. Scanning conditions: (A,B) 30 mV and 30 pA; (C) 10 mV and 50 nA.

DOI: 10.1021/jacs.6b03339
J. Am. Chem. Soc. 2016, 138, 6396−6399

Initially, we observed clusters of mobile depressions on the Cu terraces, previously identified as H adatoms due to their characteristic diffusion rate at 5 K on Cu (Figure 2A).[22] Increasing the bias applied to the STM tip removed these H atoms (Figure 2B). Select immobile depressions remained on the surface that could only be removed by individual pulses locally delivered by the STM tip (5 V) (Figure 2C); hence, the dark, immobile depressions are CO molecules, as also previously reported.[23] After removal of the CO molecules, stationary surface protrusions were observed where the CO molecules were previously located. We identify the ~20 pm high protrusions as Pt atoms substituted into the Cu lattice, thus providing further evidence of the selective adsorption of CO on the Pt sites. These STM experiments also demonstrate that H adatoms are capable of diffusing onto Cu sites and away from the Pt dissociation sites, yielding H atom coverage of 0.1 ML from 0.01 ML Pt.

Next we question, how does the weaker CO-Pt binding on Pt-Cu SAA contribute to its CO tolerance? We conducted H_2–D_2 exchange experiments to evaluate the effect of CO on H_2 activation on Pt-Cu SAAs and monometallic Pt catalysts. The mobility of H atoms on Pt-Cu SAAs was demonstrated in UHV by co-adsorption of H_2 and D_2 onto SAA Pt-Cu(111) (Figure 3A). We observed desorption of HD (m/z = 3), which provides

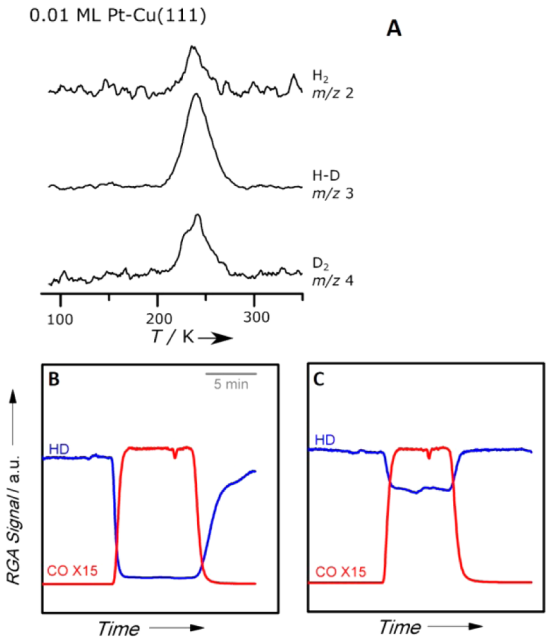

Figure 3. (A) H-D scrambling on a model Pt-Cu(111) SAA surface. Desorption traces are shown resulting from adsorption of equivalent amounts of H_2 and D_2. Real catalyst data for isothermal H_2–D_2 exchange over (B) Pt-NP and (C) $Pt_{0.008}$Cu-SAA at 150 °C. Gas composition: 33% H_2, 33% D_2, 3.3% CO, and balance argon; total flow rate, 50 mL/min; 90 mg catalyst load. Same Pt loading was applied in both samples (Table S1).

evidence of the dissociation of H_2 and migration of H atoms away from the dissociation site. When equal amounts of H and D atoms are adsorbed on the surface, we observe complete scrambling of H and D, with an H_2:HD:D_2 ratio of 1:2:1 due to H atom spillover and the facile diffusion on Cu.

Extending this common principle, H_2–D_2 exchange was employed to characterize the H_2 dissociation activity on the corresponding nanocatalysts at ambient pressure in a flow reactor setup. As shown in Figure 3B,C, HD is initially produced when H_2 and D_2 are co-fed into the reactor. Once CO is introduced, the HD production decreases due to CO poisoning. With the same CO concentration in the gas phase, $Pt_{0.008}$Cu-SAA yields 12 times more HD than Pt-NP at 150 °C. Since the steady state CO coverage is a function of binding strength, and we have shown that CO binds to Pt-Cu SAAs more weakly compared to pure Pt, the reduced binding strength of CO to $Pt_{0.008}$Cu-SAA yields more CO-free sites that are available for H_2 activation and hence HD production.

To investigate the CO tolerance of Pt-Cu SAA under realistic catalytic reaction conditions, we conducted the selective hydrogenation of acetylene over $Pt_{0.008}$Cu-SAA and Pt-NP, with and without CO in a flow reactor. We found about half of the reaction rate was retained for $Pt_{0.008}$Cu-SAA with 200 ppm CO, which is a typical CO concentration found in industrial H_2 gas (Figures 4 and S4). However, the hydrogenation activity of

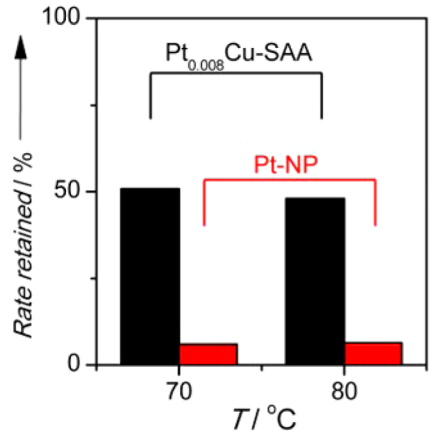

Figure 4. Ratio of retained reaction rate of acetylene hydrogenation in CO over $Pt_{0.008}$Cu-SAA and Pt-NP at different temperatures. Rate retained = reaction rate with CO/rate without CO in the reaction gas. Gas composition: 20% H_2, 2.2% C_2H_2, 200 ppm of CO, 10% argon, and balance He.

Pt-NP decreased 15-fold with 200 ppm CO. The H_2–D_2 exchange and acetylene hydrogenation activity of Cu-NP were at least 1 order of magnitude lower than those of $Pt_{0.008}$Cu-SAA at these temperatures. Our results demonstrate that Pt-Cu SAAs offer a new approach to design CO-tolerant materials for industrial applications.

To summarize, we investigated the fundamentals of CO adsorption on Pt-Cu alloys using a variety of surface science and catalysis techniques. We found that CO binds more weakly to single Pt atoms in Cu compared to larger Pt ensembles or monometallic Pt. Thus, when CO is present in the gas phase, more CO-free Pt sites are available on the SAA than the monometallic Pt, yielding higher H_2 activation reactivity and sequential hydrogenation activity under realistic conditions, which we demonstrated for SAA catalysts. We postulate that this SAA approach in other metal combinations can be used for the design of novel CO-tolerant catalysts for other industrially important reactions, such as hydrocarbon and alcohol oxidation reactions, and for the current-generation, low-temperature hydrogen fuel cells, where the Pt electrocatalysts are prone to CO poisoning.

DOI: 10.1021/jacs.6b03339
J. Am. Chem. Soc. 2016, 138, 6396–6399

■ ASSOCIATED CONTENT

Supporting Information

The Supporting Information is available free of charge on the ACS Publications website at DOI: 10.1021/jacs.6b03339.

Experimental methods, additional infrared spectroscopy, isothermal exchange of H_2 and D_2, hydrogenation of acetylene, and EXAFS characterization (PDF)

■ AUTHOR INFORMATION

Corresponding Authors

*maria.flytzani-stephanopoulos@tufts.edu

*charles.sykes@tufts.edu

Author Contributions

⊥J.L. and F.R.L. contributed equally.

Notes

The authors declare no competing financial interest.

■ ACKNOWLEDGMENTS

We dedicate this work to the memory of Howard Saltsburg. We thank the National Science Foundation (CBET-1159882 to J.L.), and the U.S. Department of Energy (DE-FG02-05ER15730 to A.J.T. and M.F-S. and DE-FG02-10ER16170 to F.R.L. and E.C.H.S.) for the financial support of this work. M.D.M. thanks the Tufts University Department of Chemistry for an Illumina Fellowship. J.L. thanks Prof. Terry Haas (Tufts University) for assistance with the IR analysis. The XAS research used resources of the Advanced Photon Source, a U.S. Department of Energy (DOE), Office of Science, User Facility operated for the DOE Office of Science by Argonne National Laboratory under Contract No. DE-AC02-06CH11357.

■ REFERENCES

(1) Cheng, X.; Shi, Z.; Glass, N.; Zhang, L.; Zhang, J.; Song, D.; Liu, Z.; Wang, H.; Shen, J. *J. Power Sources* **2007**, *165*, 739−756.

(2) Baschuk, J. J.; Li, X. *Int. J. Energy Res.* **2001**, *25*, 695−713.

(3) Zhai, Y.; Pierre, D.; Si, R.; Deng, W.; Ferrin, P.; Nilekar, A. U.; Peng, G.; Herron, J. A.; Bell, D. C.; Saltsburg, H.; Mavrikakis, M.; Flytzani-Stephanopoulos, M. *Science* **2010**, *329*, 1633−1636.

(4) Yang, M.; Liu, J.; Lee, S.; Zugic, B.; Huang, J.; Allard, L. F.; Flytzani-Stephanopoulos, M. *J. Am. Chem. Soc.* **2015**, *137*, 3470−3473.

(5) Kistler, J. D.; Chotigkrai, N.; Xu, P.; Enderle, B.; Praserthdam, P.; Chen, C. Y.; Browning, N. D.; Gates, B. C. *Angew. Chem., Int. Ed.* **2014**, *53*, 8904−8907.

(6) Peterson, E. J.; DeLaRiva, A. T.; Lin, S.; Johnson, R. S.; Guo, H.; Miller, J. T.; Kwak, J. H.; Peden, C. H. F.; Kiefer, B.; Allard, L. F.; Ribeiro, F. H.; Datye, A. K. *Nat. Commun.* **2014**, *5*, 4885.

(7) Qiao, B.; Wang, A.; Yang, X.; Allard, L. F.; Jiang, Z.; Cui, Y.; Liu, J.; Li, J.; Zhang, T. *Nat. Chem.* **2011**, *3*, 634−641.

(8) Vilé, G.; Albani, D.; Nachtegaal, M.; Chen, Z.; Dontsova, D.; Antonietti, M.; López, N.; Pérez-Ramírez, J. *Angew. Chem., Int. Ed.* **2015**, *54* (38), 11265−11269.

(9) Kyriakou, G.; Boucher, M. B.; Jewell, A. D.; Lewis, E. A.; Lawton, T. J.; Baber, A. E.; Tierney, H. L.; Flytzani-Stephanopoulos, M.; Sykes, E. C. H. *Science* **2012**, *335*, 1209−1212.

(10) Boucher, M. B.; Zugic, B.; Cladaras, G.; Kammert, J.; Marcinkowski, M. D.; Lawton, T. J.; Sykes, E. C. H.; Flytzani-Stephanopoulos, M. *Phys. Chem. Chem. Phys.* **2013**, *15*, 12187−12196.

(11) Lucci, F. R.; Liu, J.; Marcinkowski, M. D.; Yang, M.; Allard, L. F.; Flytzani-Stephanopoulos, M.; Sykes, E. C. H. *Nat. Commun.* **2015**, *6*, 8550.

(12) Boucher, M. B.; Marcinkowski, M. D.; Liriano, M. L.; Murphy, C. J.; Lewis, E. A.; Jewell, A. D.; Mattera, M. F. G.; Kyriakou, G.; Flytzani-Stephanopoulos, M.; Sykes, E. C. H. *ACS Nano* **2013**, *7*, 6181−6187.

(13) Shan, J.; Lucci, F. R.; Liu, J.; El-Soda, M.; Marcinkowski, M. D.; Allard, L. F.; Sykes, E. C. H.; Flytzani-Stephanopoulos, M. *Surf. Sci.* **2016**, DOI: 10.1016/j.susc.2016.02.010.

(14) Lucci, F. R.; Marcinkowski, M. D.; Lawton, T. J.; Sykes, E. C. H. *J. Phys. Chem. C* **2015**, *119* (43), 24351−24357.

(15) Pedersen, M. Ø.; Helveg, S.; Ruban, A.; Stensgaard, I.; Lægsgaard, E.; Nørskov, J. K.; Besenbacher, F. *Surf. Sci.* **1999**, *426*, 395−409.

(16) Ruff, M.; Takehiro, N.; Liu, P.; Nørskov, J. K.; Behm, R. J. *ChemPhysChem* **2007**, *8*, 2068−2071.

(17) Kirstein, W.; Krüger, B.; Thieme, F. *Surf. Sci.* **1986**, *176*, 505−529.

(18) Lucci, F. R.; Lawton, T. J.; Pronschinske, A.; Sykes, E. C. H. *J. Phys. Chem. C* **2014**, *118*, 3015−3022.

(19) Collins, D. M.; Spicer, W. E. *Surf. Sci.* **1977**, *69*, 85−113.

(20) Castro, G. R.; Doyen, G. *Surf. Sci.* **1994**, *307*, 384.

(21) Zhang, C. J.; Baxter, R. J.; Hu, P.; Alavi, A.; Lee, M. H. *J. Chem. Phys.* **2001**, *115* (11), 5272.

(22) Jewell, A. D.; Peng, G.; Mattera, M. F. G.; Lewis, E. A.; Murphy, C. J.; Kyriakou, G.; Mavrikakis, M.; Sykes, E. C. H. *ACS Nano* **2012**, *6*, 10115−10121.

(23) Bartels, L.; Meyer, G.; Rieder, K.-H.; Velic, D.; Knoesel, E.; Hotzel, A.; Wolf, M.; Ertl, G. *Phys. Rev. Lett.* **1998**, *80*, 2004−2007.

DOI: 10.1021/jacs.6b03339
J. Am. Chem. Soc. 2016, 138, 6396−6399